Automatica 46 (2010) 452–459

Contents lists available at ScienceDirect

Automatica

journal homepage: www.elsevier.com/locate/automatica

Brief paper

Speed regulation in steering-based source seeking ☆

Nima Ghods, Miroslav Krstic *

Department of Mechanical and Aerospace Engineering, University of California, San Diego, La Jolla, CA 92093-0411, USA

ARTICLE INFO

Article history:
Received 14 July 2009
Received in revised form
23 October 2009
Accepted 16 November 2009
Available online 5 December 2009

Keywords:
Extremum seeking
Adaptive control
Nonholonomic unicycle
Autonomous agents
Averaging

ABSTRACT

The simplest strategy for extremum seeking-based source localization, for sources with unknown spatial distributions and nonholonomic unicycle vehicles without position measurement, employs a constant positive forward speed. Steering of the vehicle in the plane is performed using only the variation of the angular velocity. While keeping the forward speed constant is a reasonable strategy motivated by implementation with aerial vehicles, it leads to complexities in the asymptotic behavior of the vehicle, since the vehicle cannot settle—at best it can converge to a small-size attractor around the source. In this paper we regulate the forward velocity, with the intent of bringing the vehicle to a stop, or as close to a stop as possible. The vehicle speed is controlled using simple derivative-like feedback of the sensor measurement (the derivative is approximated with a washout filter) to which a speed bias parameter V_c is added. The angular velocity is tuned using standard extremum seeking. We prove two results. For V_c in a certain range around zero, we show that the vehicle converges to a ring around the source and on average the limit of the vehicle's heading is either directly away or towards the source. For other values of $V_c > 0$, the vehicle converges to a ring around the source and it revolves around the source. Interestingly, the average heading of this revolution around the source is more outward than inward—this is possible because the vehicle's speed is not constant, it is lower during the outward steering intervals and higher during the inward steering intervals. The theoretical results are illustrated with simulations.

1. Introduction

Motivation. In the rapidly growing literature on coordinated motion control and autonomous agents, "autonomous" never means deprivation of position information. The vehicles are always assumed to have global positioning system (GPS) and/or inertial navigation system (INS) on board. There is, however, interest in developing vehicles with greater autonomy, free of position measurements. The reasons are two-fold: (1) applications underwater, under ice, or in buildings and "urban canyons" where GPS is unavailable, and (2) the high cost of INS systems that remain accurate over extended periods of time.

In previous papers, (Cochran & Krstic, 2007; Zhang, Arnold, Ghods, Siranosian, & Krstic, 2007), we considered the problem of seeking the source of a scalar signal using a nonholonomic vehicle with no position information. We designed two distinct strategies—keeping the angular velocity constant and tuning the forward speed by extremum seeking (Zhang et al., 2007); and keeping the forward speed constant and tuning the angular velocity by extremum seeking (Cochran & Krstic, 2007). The strategy in Zhang et al. (2007) generates vehicle motions that resemble triangles, rhombi, or stars (with arc-shaped sides), which drift towards the source, resulting in periodic motions around the source. The strategy in Cochran and Krstic (2007) generates motions that sinusoidally converge towards the source and settle into an *almost periodic* (in a mathematical sense of the term) motion in a ring around the source. While the proof of the result (Cochran & Krstic, 2007) is more challenging, the vehicle motion is much more efficient than with the strategy in Zhang et al. (2007), since the simple tuning of the heading results in trajectories where the distance of the vehicle from the source decreases monotonically.

Contribution. Neither of the strategies in Cochran and Krstic (2007) and Zhang et al. (2007) are ideal, since Zhang et al. (2007) sacrifice the transients, whereas Cochran and Krstic (2007) complexify the asymptotic performance. In this paper we aim for the best of both worlds, but not by simply combining the strategies in Cochran and Krstic (2007) and Zhang et al. (2007). We propose something more elegant, a strategy that partly simplifies the approach in Cochran and Krstic (2007), while adding a simple derivative-like feedback to a nominal forward speed V_c. This feedback allows the vehicle to slow down as it gets closer to the source and converge closer to the source without giving up convergence speed.

☆ This work was supported by Los Alamos National Laboratory and Office of Naval Research (ONR). This paper was not presented at any IFAC meeting. This paper was recommended for publication in revised form by Associate Editor Warren E. Dixon under the direction of Editor Andrew R. Teel.

* Corresponding author. Tel.: +1 858 822 1374; fax: +1 858 822 3107.
E-mail addresses: nghods@ucsd.edu (N. Ghods), krstic@ucsd.edu (M. Krstic).

0005-1098/$ – see front matter © 2009 Elsevier Ltd. All rights reserved.
doi:10.1016/j.automatica.2009.11.023

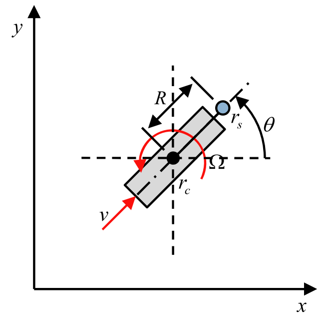

Fig. 1. The notation used in the model of vehicle sensor and center dynamics.

We prove two results, for quadratic signal fields that decay with the distance from the source. For V_c in a certain range around zero, we show that the vehicle converges to a ring around the source and on average the limit of the vehicle's heading is either directly away or towards the source. For other values of $V_c > 0$, the vehicle converges to a ring around the source and it revolves around the source. Interestingly, the average heading of this revolution around the source is more outward than inward—this is possible because the vehicle's speed is not constant, it is lower during the outward steering intervals and higher during the inward steering intervals. The theoretical results are illustrated with simulations. A simulation is also done to consider that case of Rosenbrock function as the signal field.

Source Seeking and Prior Literature. Multi-agent and GPS-enabled source seeking problems have been solved in Ogren, Fiorelli, and Leonard (2004) and Porat and Neohorai (1996). Realistic source seeking formulations require incorporation of non-holonomic constraints on the vehicle models. Such constraints are present in the standard unicycle model, which has been the basis of numerous studies in vehicle formation control, including Justh and Krishnaprasad (2004), Klein and Morgansen (2006) and Marshall, Broucke, and Francis (2006). The level set tracing work in Baronov and Baillieul (2008) is also based on the unicycle model. A hybrid strategy for solving the source seeking problem was developed in Mayhew, Sanfelice, and Teel (2008). The key tool in the present work is extremum seeking (Ariyur & Krstic, 2003), which has been advanced or employed in applications by several other authors Adetola and Guay (2007), Biyik and Arcak (2008), Centioli et al. (2005), King et al. (2006), Li, Rotea, Chiu, Mongeau, and Paek (2005), Ou et al. (2007), Peterson and Stefanopoulou (2004), Popovic, Jankovic, Magner, and Teel (2006), Stegath, Sharma, Gregory, and Dixon (2007), Tan, Nesic, and Mareels (2006), Tanelli, Astolfi, and Savaresi (2006), Wang, Yeung, and Krstic (1999), Wang and Krstic (2000) and Zhang, Dawson, Dixon, and Xian (2006).

Organization of the Paper. We start the paper in Section 2 with a description of the vehicle model and extremum seeking scheme. We derive the averaged system in Section 3. We prove local exponential convergence results to ring/annulus-shaped sets around the source in Sections 4 and 5. Section 4 deals with the case of small $|V_c|$, whereas Section 5 deals with medium and large positive values of V_c. Simulation results in Sections 4 and 5 illustrate the distinct behaviors exhibited using different values of V_c. In Section 6 we summarize the set of possible motions and attractors near the source that are achieved for different values of a key design parameter.

2. Vehicle model and control design

We consider a mobile agent modeled as a unicycle with a sensor mounted at a distance R away from the center. The diagram in Fig. 1 depicts the position, heading, angular and forward velocities for

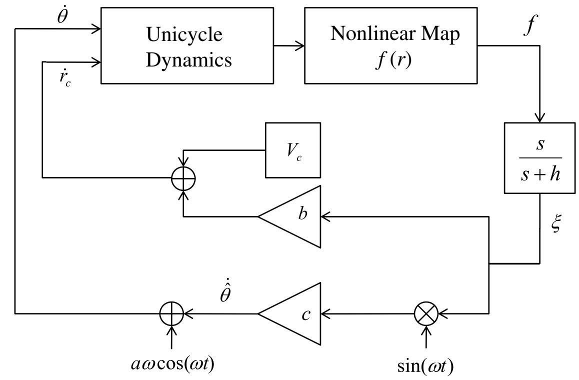

Fig. 2. Block diagram of source seeking via tuning of angular velocity and forward velocity using one reading.

the center and sensor. The equations of motion for the vehicle's center are

$$\dot{r}_c = v e^{j\theta} \tag{1}$$

$$\dot{\theta} = \Omega \tag{2}$$

where r_c is complex variable that represents the center of the vehicle in 2D, θ is the orientation and v and Ω are the forward and angular velocity inputs, respectively. The sensor is located at $r_s = r_c + Re^{j\theta}$. Note that this convenient complex representation of the position would be less useful if extending this work to a 3D setting.

The task of the vehicle is to seek a source that emits a signal (for example, the concentration of a chemical, biological agent, electromagnetic, acoustic, or even thermal signal) which decays as a function of distance away from the source. We assume this signal field is distributed according to an unknown nonlinear map $f(r(x, y))$ which has an isolated local maximum $f^* = f(r^*)$ where r^* is the location of the local maximum. We design a controller that achieves local convergence to r^* without knowledge of the shape of f, using only the measurement $f(r_s)$.

We employ extremum seeking to tune the angular velocity (Ω) directly and the forward velocity (v) indirectly. This scheme is depicted by the block diagram in Fig. 2. The control laws are given by

$$\Omega = a\omega\cos(\omega t) + c\xi\sin(\omega t) \tag{3}$$

$$v = V_c + b\xi, \tag{4}$$

where ξ is the output of the washout filter, namely, of the approximate differentiator of $f(r_s, t)$. The performance can be influenced by the parameters a, c, b, R, h, ω and V_c. We tune angular velocity Ω with the basic extremum seeking tuning law, which has a perturbation term, $a\omega\cos(\omega t)$, to excite the system. The $\xi\sin(\omega t)$ term estimates the angular gradient of the map.

The forward velocity $v = V_c + b\xi$ is chosen using the following intuition. When the vehicle is approaching the source, heading straight towards it, the sensor reading is increasing and hence $\xi > 0$. It is reasonable to speed up the vehicle when it is going towards the source. Conversely, when the vehicle is past the source and the signal reading is decreasing, i.e., $\xi < 0$, the vehicle should be slowed down, which (4) achieves.

We stress that the steering feedback (3) does not employ the nonlinear damping introduced in Cochran and Krstic (2007). The damping needed to exponentially stabilize the average equilibria is provided by the forward speed feedback (4).

3. The average system

We focus on maps which depend on the distance from the source only. Since our goal is only the establishment of local convergence, we assume that the map is quadratic, namely,

$$f(r_s) = f^* - q_r|r_s - r^*|^2 \tag{5}$$

where r^* is the unknown maximizer, $f^* = f(r^*)$ is the unknown maximum and q_r is an unknown positive constant.

We define an output error variable

$$e = \frac{h}{s+h}[f] - f^*, \tag{6}$$

where $\frac{h}{s+h}[f]$ is a low-pass filter applied to the sensor reading f, which allows us to express ξ, the output of the washout filter, as $\xi = \frac{s}{s+h}[f] = f(r_s) - \frac{h}{s+h}[f] = f(r_s - f^* - e)$, noting also that $\dot{e} = h\xi$.

Consider the system

$$\dot{r}_c = (V_c + b\xi)\mathrm{e}^{j\theta} \tag{7}$$

$$\dot{\theta} = a\omega\cos(\omega t) + c\xi\sin(\omega t) \tag{8}$$

$$\dot{e} = h\xi \tag{9}$$

$$\xi = -(q_r|r_s - r^*|^2 + e) \tag{10}$$

$$r_s = r_c + R\mathrm{e}^{j\theta} \tag{11}$$

shown in Fig. 2. To analyze this system we start by defining the shifted variables

$$\hat{r}_c = r_c - r^* \tag{12}$$

$$\hat{\theta} = \theta - a\sin(\omega t) \tag{13}$$

$$\hat{e} = e - q_r R^2. \tag{14}$$

We also introduce the time scale change

$$\tau = \omega t, \tag{15}$$

and introduce a map from the position $\hat{r}_c$ to a scalar quantity θ^*, given by

$$-\hat{r}_c = |\hat{r}_c|\mathrm{e}^{j\theta^*} \tag{16}$$

$$\theta^* = -\frac{j}{2}\ln\left(-\frac{\hat{r}_c}{\bar{\hat{r}}_c}\right) = \arg(r^* - r_c), \tag{17}$$

where θ^* represents the heading angle *towards* the source located at r^* when the vehicle is at r_c, and $\bar{\hat{r}}_c$ is the complex conjugate of $\hat{r}_c$. Using these definitions, the expression for ξ is

$$\begin{aligned}\xi &= -\left(q_r|r_c + R\mathrm{e}^{j\theta} - r^*|^2 + \hat{e} - q_r R^2\right)\\ &= -\left(q_r\left(|\hat{r}_c|^2 - 2R|\hat{r}_c|\cos(\hat{\theta} - \theta^* + a\sin(\tau))\right) + \hat{e}\right).\end{aligned} \tag{18}$$

The dynamics of the shifted system are

$$\frac{\mathrm{d}\hat{r}_c}{\mathrm{d}\tau} = \frac{1}{\omega}\left\{(V_c + b\xi)\mathrm{e}^{j(\hat{\theta} + a\sin(\tau))}\right\} \tag{19}$$

$$\frac{\mathrm{d}\hat{\theta}}{\mathrm{d}\tau} = \frac{1}{\omega}c\xi\sin(\tau) \tag{20}$$

$$\frac{\mathrm{d}\hat{e}}{\mathrm{d}\tau} = \frac{1}{\omega}h\xi. \tag{21}$$

We next define error variables $\tilde{r}_c$ and $\tilde{\theta}$ (depicted in Fig. 3), which represent the distance to the source, and the difference between the vehicle's heading and the optimal heading, respectively,

$$\tilde{r}_c = |\hat{r}_c| \tag{22}$$

$$\tilde{\theta} = \hat{\theta} - \theta^*. \tag{23}$$

The resulting dynamics for the error variables are

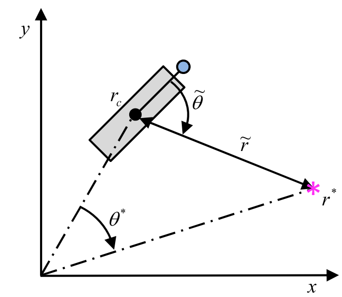

Fig. 3. Diagram of the error variables relating the vehicle and the source.

$$\begin{aligned}\frac{\mathrm{d}\tilde{r}_c}{\mathrm{d}\tau} &= \frac{\mathrm{d}\sqrt{\hat{r}_c\bar{\hat{r}}_c}}{\mathrm{d}\tau} = \frac{1}{2|\hat{r}_c|}\left(\frac{\mathrm{d}\hat{r}_c}{\mathrm{d}\tau}\bar{\hat{r}}_c + \hat{r}_c\frac{\mathrm{d}\bar{\hat{r}}_c}{\mathrm{d}\tau}\right)\\ &= -\frac{V_c + b\xi}{\omega}\cos\left(\tilde{\theta} + a\sin(\tau)\right)\end{aligned} \tag{24}$$

$$\begin{aligned}\frac{\mathrm{d}\tilde{\theta}}{\mathrm{d}\tau} &= \frac{\mathrm{d}\hat{\theta}}{\mathrm{d}\tau} - \frac{\mathrm{d}\theta^*}{\mathrm{d}\tau} = \frac{\mathrm{d}\hat{\theta}}{\mathrm{d}\tau} + \frac{j}{2|\hat{r}_c|^2}\left(\frac{\mathrm{d}\hat{r}_c}{\mathrm{d}\tau}\bar{\hat{r}}_c - \hat{r}_c\frac{\mathrm{d}\bar{\hat{r}}_c}{\mathrm{d}\tau}\right)\\ &= \frac{1}{\omega}\left[c\xi\sin(\tau) + \frac{V_c + b\xi}{\tilde{r}_c}\sin\left(\tilde{\theta} + a\sin(\tau)\right)\right]\end{aligned} \tag{25}$$

$$\frac{\mathrm{d}\hat{e}}{\mathrm{d}\tau} = \frac{1}{\omega}h\xi \tag{26}$$

$$\xi = -\left(q_r\tilde{r}_c^2 + \hat{e} - 2q_r R\tilde{r}_c\cos\left(\tilde{\theta} + a\sin(\tau)\right)\right). \tag{27}$$

The system of equations is periodic with a period 2π, and the averaged error system is

$$\begin{aligned}\frac{\mathrm{d}\tilde{r}_c^{\mathrm{ave}}}{\mathrm{d}\tau} = \frac{1}{\omega}\Big[& bJ_0(a)(q_r\tilde{r}_c^{\mathrm{ave}^2} + \hat{e}^{\mathrm{ave}})\cos(\tilde{\theta}^{\mathrm{ave}}) - bq_r R\tilde{r}_c^{\mathrm{ave}}\\ &\times(1 + J_0(2a)\cos(2\tilde{\theta}^{\mathrm{ave}})) - V_c J_0(a)\cos(\tilde{\theta}^{\mathrm{ave}})\Big]\end{aligned} \tag{28}$$

$$\begin{aligned}\frac{\mathrm{d}\tilde{\theta}^{\mathrm{ave}}}{\mathrm{d}\tau} = \frac{1}{\omega}\Big[& -q_r(2cRJ_1(a) + bJ_0(a))\tilde{r}_c^{\mathrm{ave}}\sin(\tilde{\theta}^{\mathrm{ave}}) + bq_r RJ_0(2a)\\ &\times\sin(2\tilde{\theta}^{\mathrm{ave}}) + \frac{V_c J_0(a) - bJ_0(a)\hat{e}^{\mathrm{ave}}}{\tilde{r}_c}\sin(\tilde{\theta}^{\mathrm{ave}})\Big]\end{aligned} \tag{29}$$

$$\frac{\mathrm{d}\hat{e}^{\mathrm{ave}}}{\mathrm{d}\tau} = \frac{-h}{\omega}\left[(q_r\tilde{r}_c^{\mathrm{ave}^2} + \hat{e}^{\mathrm{ave}}) - 2q_r RJ_0(a)\tilde{r}_c^{\mathrm{ave}}\cos(\tilde{\theta}^{\mathrm{ave}})\right], \tag{30}$$

where $J_1(a)$ and $J_1(a)$ are Bessel functions of the first kind. The averaged error system (28)–(30) has four equilibria defined by

$$\begin{cases}\tilde{r}_c^{\mathrm{ave}^{\mathrm{eq}1}} &= \dfrac{V_c J_0(a)}{bq_r R\rho_1}\\ \tilde{\theta}^{\mathrm{ave}^{\mathrm{eq}1}} &= \pi\\ \hat{e}^{\mathrm{ave}^{\mathrm{eq}1}} &= e_{12},\end{cases} \tag{31}$$

$$\begin{cases}\tilde{r}_c^{\mathrm{ave}^{\mathrm{eq}2}} &= -\dfrac{V_c J_0(a)}{bq_r R\rho_1}\\ \tilde{\theta}^{\mathrm{ave}^{\mathrm{eq}2}} &= 0\\ \hat{e}^{\mathrm{ave}^{\mathrm{eq}2}} &= e_{12},\end{cases} \tag{32}$$

$$\begin{cases}\tilde{r}_c^{\mathrm{ave}^{\mathrm{eq}3}} &= \rho_0\\ \tilde{\theta}^{\mathrm{ave}^{\mathrm{eq}3}} &= \pi + \mu_0\\ \hat{e}^{\mathrm{ave}^{\mathrm{eq}3}} &= e_{34}\end{cases} \tag{33}$$

$$\begin{cases}\tilde{r}_c^{\mathrm{ave}^{\mathrm{eq}4}} &= \rho_0\\ \tilde{\theta}^{\mathrm{ave}^{\mathrm{eq}4}} &= \pi - \mu_0\\ \hat{e}^{\mathrm{ave}^{\mathrm{eq}4}} &= e_{34},\end{cases} \tag{34}$$

where

$$\rho_0 = \frac{\sqrt{\gamma_1}}{\sqrt{2}cJ_1(a)} \tag{35}$$

$$\mu_0 = \arctan\frac{\sqrt{\gamma_2}}{b\sqrt{q_r R}(1-J_0(2a))} \tag{36}$$

$$e_{12} = -\frac{2V_c J_0^2(a)}{b\rho_1} - \frac{(V_c J_0^2(a))^2}{q_r b^2 R^2 \rho_1^2} \tag{37}$$

$$e_{34} = -\frac{\gamma_1}{2c^2 R J_1^2(a)} \tag{38}$$

$$+\frac{bq_r RhJ_0(a)\sqrt{2\gamma_1}(1-J_0(2a))}{cJ_1(a)\sqrt{\gamma_2+b^2q_rR(1-J_0(2a))^2}}. \tag{39}$$

and

$$\gamma_1 = cJ_1(a)J_0(a)V_c + b^2 q_r R\rho_2$$
$$\gamma_2 = 2cJ_1(a)J_0(a)V_c - b^2 q_r R\rho_3$$
$$\rho_1 = 1 + J_0(2a) - 2J_0^2(a) \geq 0$$
$$\rho_2 = J_0^2(a) - J_0(2a) - J_0(2a)J_0^2(a) + J_0^2(2a)$$
$$\rho_3 = -2J_0^2(a) + 2J_0(2a)J_0^2(a) - J_0^2(2a) + 1 \geq 0.$$

Note that, due to the properties of Bessel functions, $1 - J_0(2a)$ is positive for all positive a. In addition, $\rho_1(a)$ and $\rho_3(a) = (1 - J_0(2a))\rho_1(a)$ are positive for all positive and sufficiently small values of a. In fact, both $\rho_1(a)$ and $\rho_3(a) > 0$ appear to be positive for *all* positive values of a (rather than only for small $a > 0$), but this may be difficult to prove.

Due to the transformation (22), the four equilibria (31)–(34) can only be related back to the original system if $\tilde{r}_c^{\text{ave}}$ is real and positive. It should be noted that $\tilde{r}_c^{\text{ave}^{\text{eq1}}}$ and $\tilde{r}_c^{\text{ave}^{\text{eq2}}}$ cannot simultaneously be positive (note that V_c can be either positive or negative), and also that $\tilde{r}_c^{\text{ave}^{\text{eq3}}}$ and $\tilde{r}_c^{\text{ave}^{\text{eq4}}}$ are real only when $\gamma_1 > 0$. In the next two sections we will show stability of the four average equilibria (not all of them simultaneously) for different values of the speed bias parameter V_c, and infer the appropriate convergence properties for the non-average system (24)–(27).

Each four of the average equilibria (31)–(34) represents a ring around the source. However, more interesting information is obtained when considering the average values of $\tilde{\theta}$. With equilibrium 1 the vehicle points away from the source, with equilibrium 2 it points directly towards the source, and with equilibria 3 and 4 the vehicle points, on the average, outwards relative to the ring, revolving around the source in the counterclockwise direction for equilibrium 3 and in the clockwise direction for equilibrium 4.

4. Stability for small positive or negative V_c

In this section we analyze the stability properties of system shown in Fig. 2 when the parameter V_c is small but not zero.

Theorem 1. *Consider the system in Fig. 2 with nonlinear map (5) that has a maximum ($q_r > 0$). Let the parameters c, b, R, h be chosen as positive. Let the parameter a be chosen so that $J_0(a), J_0(2a), J_1(a), 1 + J_0(2a) - 2J_0^2(a) > 0$. Let the parameter V_c be nonzero and such that either*

$$V_c \in (0, V_c^{\text{lower}}), \tag{40}$$

where $V_c^{\text{lower}} \triangleq -\dfrac{bq_rR(1+J_0(2a))+h}{2J_0^2(a)}R\rho_1,$

or

$$V_c \in (V_c^{\text{upper}}, 0), \quad \text{where } V_c^{\text{upper}} \triangleq \frac{b^2 q_r R\rho_3}{2cJ_1(a)J_0(a)}. \tag{41}$$

There exist constants $\omega^* > 0$ and $\delta > 0$ such that, for all $\omega > \omega^*$, if the initial conditions $r_c(0), \theta(0), e(0)$ are such that

$$\left| |r_c(0) - r^*| - \frac{|V_c| J_0(a)}{bq_r R\rho_1} \right| < \delta R \tag{42}$$

$$|\theta(0) - \arg(r_c(0) - r^*) - n\pi| < \delta a, \quad n \in \mathbb{N} \tag{43}$$

$$\left| e(0) - q_r R^2 - e_{12} \right| < \delta q R^2, \tag{44}$$

then the trajectory of the vehicle center $r_c(t)$ locally exponentially converges to, and remains in, the ring

$$\frac{|V_c| J_0(a)}{bq_r R\rho_1} - O(1/\omega) \leq \left\| r_c - r^* \right\| \leq \frac{|V_c| J_0(a)}{bq_r R\rho_1} + O(1/\omega). \tag{45}$$

Proof. The Jacobian of the average system (28)–(30) at the equilibria (31) and (32) is (at both equilibria) given by

$$A^{\text{eq1}} = \frac{1}{\omega}\begin{bmatrix} \dfrac{-2V_c J_0^2(a)}{R\rho_1} - bq_r R(1+J_0(2a)) & 0 & -bJ_0(a) \\ 0 & \eta & 0 \\ -2hJ_0(a)\left(q_r R + \dfrac{V_c}{bR\rho_1}\right) & 0 & -h \end{bmatrix} \tag{46}$$

where

$$\eta = 2\frac{cJ_1(a)J_0(a)}{b\rho_1}V_c - \frac{bq_r R\rho_3}{\rho_1}. \tag{47}$$

By applying a similarity transformation with the matrix

$$T = \begin{bmatrix} 1 & 0 & 0 \\ 0 & 0 & 1 \\ 0 & 1 & 0 \end{bmatrix}, \tag{48}$$

we convert the Jacobian (46) into the block diagonal matrix

$$\text{diag}\left\{ \frac{1}{\omega}\begin{bmatrix} \dfrac{-2V_c J_0^2(a)}{R\rho_1} - bq_r R(1+J_0(2a)) & -bJ_0(a) \\ -2hJ_0(a)\left(q_r R + \dfrac{V_c}{bR\rho_1}\right) & -h \end{bmatrix}, \frac{\eta}{\omega} \right\}. \tag{49}$$

The characteristic equation for this Jacobian is the combination of the characteristic equations of the two blocks, which is

$$(\omega s)^2 + \zeta(\omega s) + hbq_r R\rho_1 = 0 \tag{50}$$

$$\omega s - \eta = 0, \tag{51}$$

where

$$\zeta = \frac{2J_0^2(a)V_c}{R\rho_1} + bq_r R(1+J_0(2a)) + h. \tag{52}$$

According to the Routh–Hurwitz criterion, to guarantee that the roots of the polynomial have negative real parts, each coefficient must be greater than zero. Hence, we need $\eta < 0$ in (47) and $\zeta > 0$ in (52). Both of these conditions are satisfied under either condition (40) or (41) of Theorem 1. By applying Theorem 10.4 from Khalil (2002) to this result, we conclude that the error system (24)–(27) has two distinct, exponentially stable periodic solutions within $O(1/\omega)$ of the equilibria (31) and (32), which proves that the vehicle center r_c converges to the annulus (45) around the source r^* defined in (45). □

Simulation: Fig. 4 shows the simulation with the map parameters $r^* = (0, 0)$, $q_r = 1$ and a vehicle initial conditions of $r_0 = (1, 1)$ and $\theta_0 = -\pi/2$. The ES parameters are chosen as $\omega = 20$, $a = 1.8$, $R = 0.1$, $c = 80$, $b = 4$, $h = 2$, and $V_c = 0.005$, which satisfies (41). Fig. 4 a, b, and c show that the error variables converge very near the theoretical equilibrium values. Fig. 4d

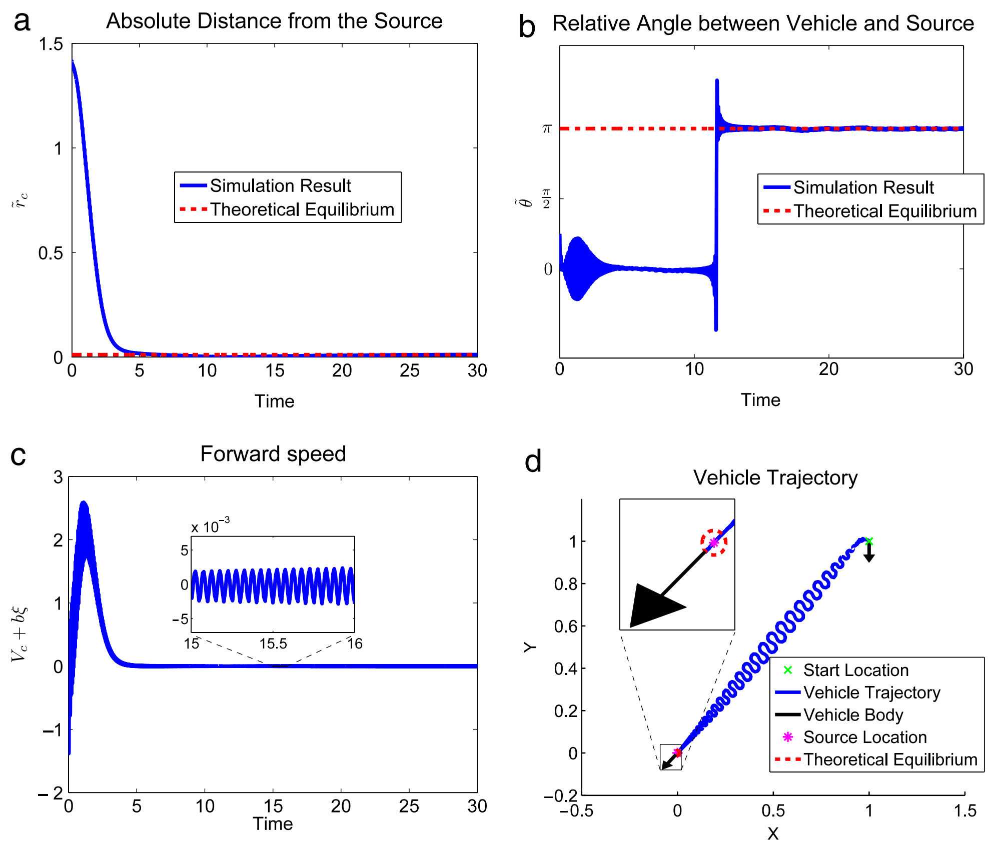

Fig. 4. Simulation results for steering-based unicycle source seeking with forward speed regulation: (a), (b), (c) showing the evolution of the variables $\tilde{r}_c$, $\tilde{\theta}$, and $V_c + b\xi$, respectively, and (d) showing the trajectory of the vehicle.

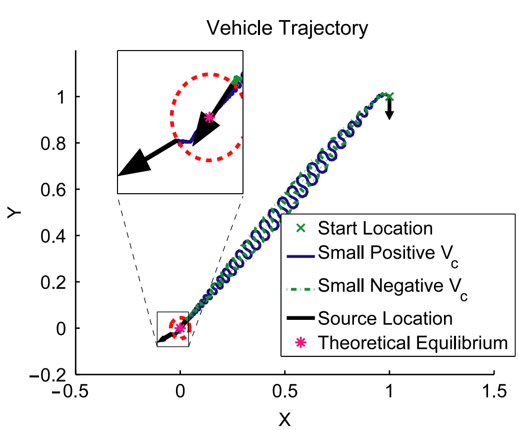

Fig. 5. The difference in trajectories for small positive and negative V_c. The two cases yield convergence to the average equilibria (31) and (32), respectively. For $V_c < 0$ the vehicle points towards the source at the end of the transient, whereas for $V_c > 0$ the vehicle points away from the source at the end of the transient.

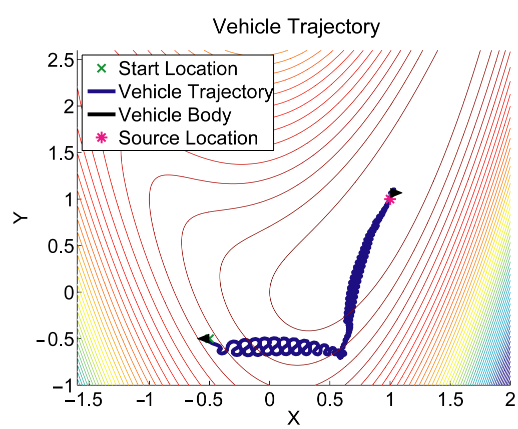

Fig. 6. Simulation result of vehicle trajectory using steering-based source seeking and forward speed regulation on a Rosenbrock function (the white shading represents the maximum).

shows the trajectory of the vehicle in the signal field. It appears from Fig. 4 d as if the vehicle comes to a full stop. This is actually not the case, as we note from the zoom frame in Fig. 4 c, and as we further explain in Remark 1.

Fig. 5 shows the main difference between the small positive and negative V_c with the map parameters, initial conditions, and ES parameters chosen to be the same as the simulation in Fig. 4 for both vehicles except for the parameter V_c, which was set to $+0.02$ for one and -0.02 for the other. While with $V_c > 0$ the vehicle heading converges to a value pointing directly away from the source, as predicted by the average equilibrium for the heading in (31), with $V_c < 0$ the vehicle heading converges to a value pointing directly towards the source, as predicted by the average equilibrium for the heading in (32).

The abilities of this extremum seeking scheme on a non-quadratic function can be seen in Fig. 6, where the vehicle can converge to the maximum with the unknown map being a Rosenbrock function. The Rosenbrock function used in Fig. 6 has a maximum at (1, 1) with the following form

$$f(r_s) = -\frac{1}{2}(1 - x_s)^2 - (y_s - x_s^2)^2, \tag{53}$$

where $x_s = \mathrm{Re}(r_s)$ and $y_s = \mathrm{Im}(r_s)$. The vehicle is given the starting positions of $r_0 = (-0.5, -0.5)$ and $\theta_0 = \pi$.The ES parameters are chosen as $\omega = 20$, $a = 1.8$, $R = 0.1$, $c = 80$, $b = 5$, $h = 1$, and $Vc = -0.005$.

Remark 1. The vehicle does not come to a full stop, as evident from Fig. 4 c, even though it slows down nearly to a stop due to a very small $V_c = 0.005$. However, unlike in Cochran and Krstic (2007), the vehicle, after entering the annulus, does not revolve around the source. It points, on the average, towards or away from the source, depending on the sign of V_c. The vehicle's angular velocity and forward speed oscillate but the vehicle does not drift clockwise or counterclockwise in the annulus. While this fact is evident from the simulations, unfortunately it cannot be proved. This is because only the *relative* heading with respect to the source has an exponentially stable equilibrium. The absolute heading, after averaging the $\hat{\theta}$-system (25), has a continuum of equilibria, but none of them are exponentially stable, which precludes the possibility of proving, using the averaging method, that no drift occurs.

Similar to Cochran and Krstic (2007), the vehicle converges to an annulus around the source with a radius proportional to V_c. From (49) we see that when h is large the decay rate in the radial state $\tilde{r}_c$ of the vehicle is a function of two terms, one with V_c and the other with b, unlike Cochran and Krstic (2007), where the convergence rate depends only on V_c, and where a trade-off between the annulus size and convergence speed exists (faster convergence implies a larger annulus, because the vehicle has constant speed). In the present design we can choose $V_c \ll b$ and achieve fast convergence to a small annulus around the source. With the choice of small V_c the vehicle comes almost to a stop, as shown in the Fig. 4.

The linearization step fails when $V_c = 0$, due to the singularity at $\tilde{r}_c = 0$ in (25). For this reason, nothing can be said about the system behavior even though $V_c = 0$ verifies the Routh–Hurwitz criterion. The singularity at $\tilde{r}_c = 0$ also manifests itself in the average equilibria (31) and (32), where $\tilde{r}_c = 0$ at both equilibria, but the heading has a non-unique value ($\tilde{\theta} = \pi$ or $\tilde{\theta} = 0$).

5. Stability for medium and large positive V_c

For medium or large values of V_c the vehicle converges to the average equilibria 3 and 4, namely to an annulus within which the vehicle revolves around the source, similar to the vehicle trajectories produced by the algorithm in Cochran and Krstic (2007). However, as we shall see, an interesting difference relative to Cochran and Krstic (2007) arises thanks to the fact that forward speed is not constant, which allows the vehicle to revolve around the source with non-tangential average heading.

Theorem 2. *Consider the system in Fig. 2 with nonlinear map (5) that has a maximum ($q_r > 0$). Let the parameters c, b, R, h be chosen as positive. Let the parameter a be chosen so that $J_0(a), J_0(2a), J_1(a), 1 + J_0(2a) - 2J_0^2(a) > 0$. Let*

$$V_c > V_c^{\text{upper}}, \tag{54}$$

where V_c^{upper} is defined in (41). There exist constants $\omega^* > 0$ and $\delta > 0$ such that, for all $\omega > \omega^*$, if the initial conditions $r_c(0), \theta(0), e(0)$ are such that

$$\left| |r_c(0) - r^*| - \frac{\sqrt{\gamma_1}}{\sqrt{2}cJ_1(a)} \right| < \delta R \tag{55}$$

$$\left| \theta(0) - \arg(r_c(0) - r^*) - (2n+1)\pi \pm \mu_0 \right| < \delta a, \quad n \in \mathbb{N} \tag{56}$$

$$\left| e(0) - q_r R^2 - e_{34} \right| < \delta q R^2, \tag{57}$$

then the trajectory of the vehicle center $r_c(t)$ locally exponentially converges to, and remains in, the annulus

$$\frac{\sqrt{\gamma_1}}{\sqrt{2}cJ_1(a)} - O(1/\omega) \le |r_c - r^*| \le \frac{\sqrt{\gamma_1}}{\sqrt{2}cJ_1(a)} + O(1/\omega). \tag{58}$$

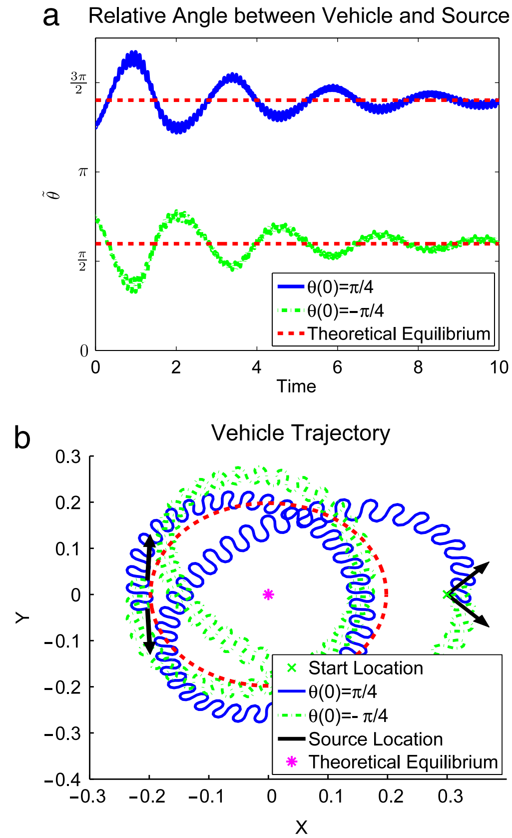

Fig. 7. Two trajectories of the same vehicle, with the only difference being the initial condition in θ. The vehicle converges to two different average equilibria, (33) and (34). (a) shows the evolution of the relative angle between the vehicle heading and the source, with $\mu_0 \approx \pi/3$. (b) shows the trajectory of the vehicles.

Proof. We first note that the condition (54) ensures that $\gamma_2 > 0$. We also note that the statement of the theorem relies on γ_1 being positive, since it appears under the square root. To see that γ_1 is indeed positive, we express it as

$$\gamma_1 = \frac{\gamma_2}{2} + b^2 q_r R \left(\frac{\rho_3}{2} + \rho_2 \right), \tag{59}$$

where

$$\frac{\rho_3}{2} + \rho_2 = \frac{1}{2} \left(1 - J_0(2a) \right)^2 \ge 0, \quad \forall a. \tag{60}$$

Since $\gamma_2 \ge 0$, it follows that $\gamma_1 > 0$ and thus it follows that the average equilibria (33) and (34) are well defined.

As done in the proof of Theorem 1, we can calculate the Jacobians for equilibria (33) and (34), which happens to be the same matrix at both equilibria. Due to the complicated form of the Jacobian matrix, we do not show the matrix and instead just show its characteristic polynomial:

$$\begin{aligned} 0 = \Bigg[(\omega s)^3 &+ \left(Rbq_r(1 + J_0(2a)) + \frac{b^2 q_r J_0(a)}{cJ_1(a)} (1 - J_0(2a)) + h \right) \\ &\times (\omega s)^2 + \left(\left(2q_r R + \frac{bq_r J_0(a)}{cJ_1(a)} \right) \gamma_2 + Rbq_r h \rho_1 \right) (\omega s) \\ &+ 2Rq_r h \gamma_2 \Bigg]. \end{aligned} \tag{61}$$

According to the Routh–Hurwitz criterion, to guarantee that the roots of the polynomial have negative real parts, each coefficient must be greater than zero and the product of the s^2 and s^1

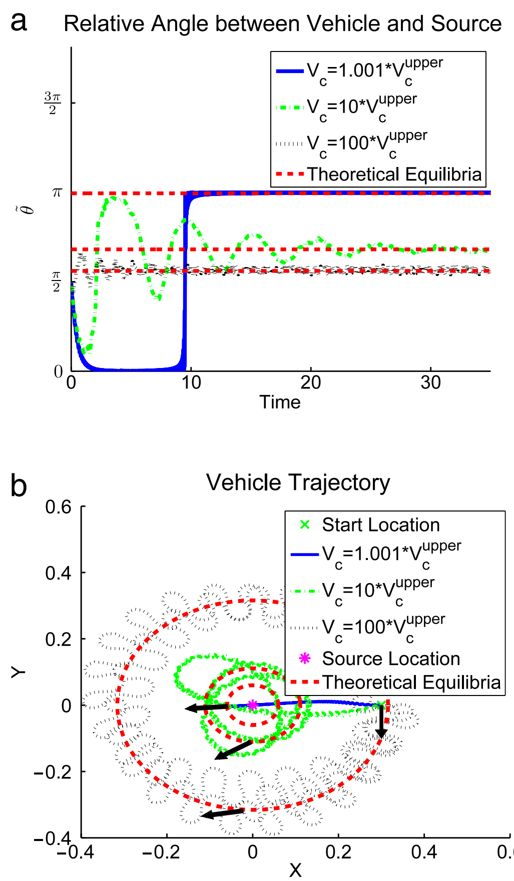

Fig. 8. Three trajectories of the same vehicle, with the only difference being the value of V_c. The vehicle converges to three different trajectories that encircle the source. (a) shows the evolution of the relative angle between the vehicle heading and the source, with $\mu_0 \approx 0$ when V_c is close to V_c^{upper} and $\mu_0 \approx \pi/2$ when $V_c \gg V_c^{\text{upper}}$. (b) shows the trajectory of the vehicles.

coefficients must be greater than the s^0 coefficient. The product of the s^2 and s^1 coefficients minus the s^0 coefficient is

$$bq_r^2\left(\left(2q_rR+\frac{bq_rJ_0(a)}{cJ_1(a)}\right)\gamma_2+Rbq_rh\rho_1\right)$$
$$\times\left(R(1+J_0(2a))+\frac{bJ_0(a)}{cJ_1(a)}(1-J_0(2a))\right)$$
$$+q_rh\left(\frac{bJ_0(a)}{cJ_1(a)}\gamma_2+Rb\rho_1\right). \tag{62}$$

With the condition (54), the Routh–Hurwitz criterion is satisfied and therefore the Jacobian for the equilibria (33) and (34) is Hurwitz. By applying Theorem 10.4 from Khalil (2002) to this result, we conclude that the error system (24)–(27) has two distinct, exponentially stable periodic solutions within $O(1/\omega)$ of the equilibria (33) and (34), which proves that the vehicle center r_c converges to the annulus (58) around the source r^*. □

Simulation: On the approach towards the source, the vehicle trajectory with $V_c > V_c^{\text{upper}}$ is very similar to the trajectory for $V_c \in (V_c^{\text{lower}}, V_c^{\text{upper}})$. However, as the vehicle for $V_c > V_c^{\text{upper}}$ gets close to the source, it begins to encircle the source clockwise or counterclockwise, depending on the initial conditions. Fig. 7 shows the simulation for $V_c > V_c^{\text{upper}}$, with two different initial conditions, one that converges to the average equilibrium (33) and the other that converges to the average equilibrium (34). The simulations in Fig. 7 were done with map parameters and the ES parameters chosen as to be the same as the simulation in Fig. 4 except for $V_c = 1$, which satisfies (54).

Fig. 8 shows a simulation of three vehicles with three different values for V_c. The simulations in Fig. 8 were done with map parameters and the ES parameters chosen to be the same as the simulation in Fig. 4 except for V_c. The three values of V_c were chosen as $1.001 \times V_c^{\text{upper}}$, $10 \times V_c^{\text{upper}}$, and $100 \times V_c^{\text{upper}}$ to show that the vehicle's average heading ranging from directly away from the source for V_c slightly larger than V_c^{upper} to almost tangential to the ring for $V_c \gg V_c^{\text{upper}}$. Note this behavior is explained by (36) and how it relates to V_c^{upper}.

6. Conclusion

We have proposed a modification of the nonholonomic source seeking algorithm in Cochran and Krstic (2007), with a regulation of the vehicle forward speed which allows the vehicle to slow down as it gets close to the source. We have proved the convergence to a neighborhood of the source in three cases, identifying three classes of attractors:

- $V_c \in (V_c^{\text{lower}}, 0)$: the vehicle points, on the average, directly towards the source, and does not drift around the ring. This is a continuum of attractors, parametrized by the position on the ring.
- $V_c \in (0, V_c^{\text{upper}})$: the vehicle points, on the average, directly away from the source, and does not drift around the ring. This is a continuum of attractors, parametrized by the position on the ring.
- $V_c > V_c^{\text{upper}}$: the vehicle revolves around the source in the clockwise or counterclockwise direction, depending on the initial condition. The vehicle's average heading ranges from slightly outward relative to the ring (for $V_c \gg V_c^{\text{upper}}$) to almost directly away from the source (for V_c only slightly larger than V_c^{upper}).

While our new strategy is not applicable to fixed-wing aircraft, it is applicable to mobile robots, marine vehicles, and rotorcraft. Of the three ranges for the speed bias parameter V_c, namely, $V_c \in (V_c^{\text{lower}}, 0)$, $V_c \in (0, V_c^{\text{upper}})$, and $V_c > V_c^{\text{upper}}$, from the point of view of asymptotic performance, the negative range $V_c \in (V_c^{\text{lower}}, 0)$ seems preferable, because the vehicle virtually stops near the source and because it points directly towards the source on average.

References

Adetola, V., & Guay, M. (2007). Parameter convergence in adaptive extremum-seeking control. *Automatica*, *43*(1), 105–110.

Ariyur, K. B., & Krstic, M. (2003). *Real time optimization by extremum seeking control*. Wiley-Interscience.

Baronov, D., & Baillieul, J. (2008). Autonomous vehicle control for ascending/descending along a potential field with two applications. In *American control conference* (pp. 678–683).

Biyik, E., & Arcak, M. (2008). Gradient climbing in formation via extremum-seeking and passivity-based coordination rules [Special issue]. In *Collective behavior and control of multi-agent systems*. *Asian J. Control*, *10*(2), 201–211.

Centioli, C., Iannone, F., Mazza, G., Panella, M., Pangione, L., & Podda, S. et al. (2005). Extremum seeking applied to the plasma control system of the frascati tokamak upgrade. In *44th IEEE conf. on decision and ctrl., and the european ctrl. conf.*.

Cochran, J., & Krstic, M. (2007). Source seeking with a nonholonomic unicycle without position measurements and with tuning of angular velocity part I: Stability analysis. In *IEEE conf. on decision and control*.

Justh, E., & Krishnaprasad, P. (2004). Equilibria and steering laws for planar formations. *Systems and Control Letters*, *52*, 25–38.

Khalil, H. (2002). *Nonlinear systems*. Prentice-Hall.

King, R., Becker, R., Feuerbach, G., Henning, L., Petz, R., & Nitsche, W. et al. (2006). Adaptive flow control using slope seeking. In *14th IEEE Mediterranean conf. on ctrl. automation*.

Klein, D., & Morgansen, K. (2006). Controlled collective motion for trajectory tracking. In *2006 American ctrl. conf*.

Li, Y., Rotea, A., Chiu, G. T.-C., Mongeau, L., & Paek, I.-S. (2005). Extremum seeking control of a tunable thermoacoustic cooler. *IEEE Trans. Contr. Syst. Technol.*, *13*, 527–536.

Marshall, J., Broucke, M., & Francis, B. (2006). Pursuit formations of unicycles. *Automatica*, *42*, 3–12.
Mayhew, C. G., Sanfelice, R. G., & Teel, A. R. (2008). Robust source-seeking hybrid controllers for nonholonomic vehicles. In *American control conference* (pp. 2722–2727).
Ogren, P., Fiorelli, E., & Leonard, N. (2004). Cooperative control of mobile sensor networks: Adaptive gradient climbing in a distributed environment. *IEEE Transactions on Automatic Control*, *29*, 1292–1302.
Ou, Y., Xu, C., Schuster, E., Luce, T., Ferron, J. R., & Walker, M. (2007). Extremum-seeking finite-time optimal control of plasma current profile at the diii-d tokamak. In *2007 American ctrl. conf.*
Peterson, K., & Stefanopoulou, A. (2004). Extremum seeking control for soft landing of an electromechanical valve actuator. *Automatica*, *29*, 1063–1069.
Popovic, D., Jankovic, M., Magner, S., & Teel, A. (2006). Extremum seeking methods for optimization of variable cam timing engine operation. *IEEE Transactions on Control Systems Technology*, *14*(3), 398–407.
Porat, B., & Neohorai, A. (1996). Localizing vapor-emitting sources by moving sensors. *IEEE Transactions on Signal Processing*, *44*, 1018–1021.
Stegath, K., Sharma, N., Gregory, C. M., & Dixon, W. E. (2007). An extremum seeking method for non-isometric neuromuscular electrical stimulation. In *IEEE international conference on systems, man and cybernetics* (pp. 2528–2532).
Tan, Y., Nesic, D., & Mareels, I. M. Y. (2006). On non-local stability properties of extremum seeking controllers. *Automatica*, *42*, 889–903.
Tanelli, M., Astolfi, A., & Savaresi, S. (2006). Non-local extremum seeking control for active braking control systems. In *Conf. on control applications*.
Wang, H.-H., & Krstic, M. (2000). Extremum seeking for limit cycle minimization. *IEEE Transactions on Automatic Control*, *45*, 2432–2436.
Wang, H.-H., Yeung, S., & Krstic, M. (1999). Experimental application of extremum seeking on an axial-flow compressor. *IEEE Transactions on Control Systems Technology*, *8*, 300–309.
Zhang, C., Arnold, D., Ghods, N., Siranosian, A. A., & Krstic, M. (2007). Source seeking with nonholonomic unicycle without position measurement and with tuning of forward velocity. *Systems & Control Letters*, *56*, 245–252.
Zhang, X. T., Dawson, D. M., Dixon, W. E., & Xian, B. (2006). Extremum seeking nonlinear controllers for a human exercise machine. *IEEE Transactions on Mechatronics*, *14*(2), 233–240.

Nima Ghods received his B.S. degree in Mechanical Engineering and his Masters degree in Aerospace Engineering from UC San Diego in 2006 and 2007, respectively. Since 2007 he has been pursuing a doctoral degree in Dynamic Systems and Control at UC San Diego. His main research activity is in the development of unmanned vehicles and the design of control algorithms for applications to tracking of distributed and spatio-temporally evolving processes. In 2008 and 2009 he led the UCSD team in the AUVSI international autonomous underwater vehicle competition. He is currently leading the autonomous vehicle efforts on two projects at UCSD, one of them on contaminant plume tracking with the Los Alamos National Laboratory and the other on olfactory sensing and localization with the Office of Naval Research.

Miroslav Krstic is the Daniel L. Alspach Professor and the founding Director of the Cymer Center for Control Systems and Dynamics (CCSD) at UC San Diego. He received his Ph.D. in 1994 from UC Santa Barbara and was Assistant Professor at University of Maryland until 1997. He is a coauthor of eight books: Nonlinear and Adaptive Control Design (Wiley, 1995), Stabilization of Nonlinear Uncertain Systems (Springer, 1998), Flow Control by Feedback (Springer, 2002), Real-time Optimization by Extremum Seeking Control (Wiley, 2003), Control of Turbulent and Magnetohydrodynamic Channel Flows (Birkhauser, 2007), Boundary Control of PDEs: A Course on Backstepping Designs (SIAM, 2008), Delay Compensation for Nonlinear, Adaptive, and PDE Systems (Birkhauser, 2009), and Adaptive Control of Parabolic PDEs (Princeton, 2010). Krstic is a Fellow of IEEE and IFAC and has received the Axelby and Schuck paper prizes, NSF Career, ONR Young Investigator, and PECASE award. He has held the appointment of Springer Distinguished Visiting Professor of Mechanical Engineering at UC Berkeley. He serves as Senior Editor in IEEE Transactions on Automatic Control and as Editor for Adaptive and Distributed Parameter Systems in Automatica. He has served as the Vice-President for Technical Activities of IEEE Control Systems Society and as the Chair of the Society's Fellow Evaluation Committee.